Carbohydrate Polymers 89 (2012) 979–991

Contents lists available at SciVerse ScienceDirect

Carbohydrate Polymers

journal homepage: www.elsevier.com/locate/carbpol

Differential effects of genetically distinct mechanisms of elevating amylose on barley starch characteristics

Ahmed Regina[a,b,*], Jaroslav Blazek[a,c], Elliot Gilbert[c], Bernadine M. Flanagan[d], Michael J. Gidley[d], Colin Cavanagh[a,b], Jean-Philippe Ral[a,b], Oscar Larroque[a,b], Anthony R. Bird[a,e], Zhongyi Li[a,b], Matthew K. Morell[a,b]

[a] CSIRO Food Futures National Research Flagship, GPO Box 1600, Canberra, ACT 2601, Australia
[b] CSIRO Plant Industry, GPO Box 1600, Canberra, ACT 2601, Australia
[c] Bragg Institute, Australian Nuclear Science and Technology Organisation, Locked Bag 2001, Kirrawee DC, NSW 2232, Australia
[d] Centre for Nutrition and Food Sciences, University of Queensland, St. Lucia, Qld 4072, Australia
[e] CSIRO Food and Nutritional Sciences, Kintore Avenue, Adelaide, SA, Australia

ARTICLE INFO

Article history:
Received 18 January 2012
Received in revised form 11 April 2012
Accepted 12 April 2012
Available online 28 April 2012

Keywords:
Amylose
Amylopectin
Barley
Starch
NMR
SAXS

ABSTRACT

The relationships between starch structure and functionality are important in underpinning the industrial and nutritional utilisation of starches. In this work, the relationships between the biosynthesis, structure, molecular organisation and functionality have been examined using a series of defined genotypes in barley with low (<20%), standard (20–30%), elevated (30–50%) and high (>50%) amylose starches. A range of techniques have been employed to determine starch physical features, higher order structure and functionality. The two genetic mechanisms for generating high amylose contents (down-regulation of branching enzymes and starch synthases, respectively) yielded starches with very different amylopectin structures but similar gelatinisation and viscosity properties driven by reduced granular order and increased amylose content. Principal components analysis (PCA) was used to elucidate the relationships between genotypes and starch molecular structure and functionality. Parameters associated with granule order (PC1) accounted for a large percentage of the variance (57%) and were closely related to amylose content. Parameters associated with amylopectin fine structure accounted for 18% of the variance but were less closely aligned to functionality parameters.

1. Introduction

Barley, a cereal crop predominantly grown for animal feed, malting and brewing applications, is increasingly gaining interest as a component of cereal-based foods for direct human consumption. In each of these applications, the starch composition is central to the functionality of the grain. As a diploid crop species that is readily transformed, barley is also of interest as a model system for investigating relationships between starch structure and functionality.

Reserve starch accounts for between 50 and 60% of the grain weight of barley. Structurally, the amylopectin and amylose fractions, the two major glucosyl polymers that constitute starch play distinct roles in granule structure and its semi-crystalline organisation. The crystalline arrays are considered to be largely comprised of ordered double helices formed by unbranched amylopectin-cluster side chains (A chains, <16 DP) and singly branched side chains (B1 chains, 20–24 DP) although more highly branched longer chains of amylopectin B2 (42–48 DP) and B3 (69–75 DP) chains are thought to pass through the crystalline array interlinking the alternating crystalline and amorphous regions (Bertoft, 2007; Bertoft, Piyachomkwan, Chatakanonda, & Sriroth, 2008; Hizukuri, 1986). In between the crystalline lamellae, amorphous amylopectin and amylose molecules are present in concentric bands, organised with a characteristic repeat distance of ca. 10 nm (Jenkins & Donald, 1995).

Depending on the hydration state and starch architecture, starch exists in several semi-crystalline forms with characteristic X-ray diffraction (XRD) patterns: A-type, B-type, C-type and V-type. Cereal starch is mainly constituted by A-type crystallinity formed by predominantly short, lateral amylopectin chains and frequent branch points (Buléon, Colonna, Planchot, & Ball, 1998). Amylopectin with longer lateral chains and less frequent branch points is associated with B-type starch. Both the A- and B-type starches consist of parallel-packed, left handed double helices, but the two differ in crystal symmetry and aspects of association of water molecules (Imberty & Perez, 1988; Wu & Sarko, 1978). C-type crystallinity is less common and contains a mixture of A- and

* Corresponding author at: CSIRO Plant Industry, GPO Box 1600, Canberra, ACT 2601, Australia. Tel.: +61 2 62465488, fax: +61 2 62465000.
E-mail address: regina.regina@csiro.au (A. Regina).

0144-8617/$ – see front matter © 2012 Elsevier Ltd. All rights reserved.
http://dx.doi.org/10.1016/j.carbpol.2012.04.054

B-types, a typical example being pea starch characterised by a central B-type and peripheral A-type structure in granules (Bogracheva, Morris, Ring, & Hedley, 1998). Amylose–lipid complexes in native starch can result in a V-type polymorph (Morrison, Law, & Snape, 1993).

Starches with altered amylose have been generated in barley either through gene mutations or gene silencing (Merritt, 1967; Morell et al., 2003; Regina, Kosar-Hashemi, Ling, Li, Rahman, & Morell, 2010) and have been characterised to some extent (Borén, Glaring, Ghebremedhin, Olsson, Blennow, & Jansson, 2008; Morell et al., 2003; Morrison, Tester, Snape, Law, & Gidley, 1993; Regina et al., 2010; Schondelmaier, Jacobi, Fischbeck, & Jahoor, 1992; Song & Jane, 2000). These include waxy starch (0–13% amylose) resulting from mutation in granule bound starch synthase (GBSS), and high amylose starches (>35%) resulting from three distinct mechanisms; the *amo1* (Merritt, 1967) mutation (amylose content up to 45% (Borén et al., 2008; Schondelmaier et al., 1992)), the starch synthase (ssIIa) mutation *Sex6* (Morell et al., 2003) and RNA mediated down-regulation of starch branching enzyme (SBE) IIa and IIb (Regina et al., 2010) with an amylose content of >70%.

The availability of the highly defined barley genotypes utilised in this study provides an opportunity to explore not only relationships between amylose content, starch structure and functionality, but also to define the impact of achieving elevated amylose content by different genetic mechanisms. In this study, starch structure has been characterised through a range of techniques defining molecular structure (chain length distribution by FACE (flurophore assisted carbohydrate electrophoresis), size exclusion chromatography of non-debranched and debranched starches), molecular organisation (^{13}CP/MAS and X-ray diffraction), and intra-granule lamellar organisation (small angle X-ray scattering). Starch thermal and functional behaviour has been explored using differential scanning calorimetry and pasting characteristics using the rapid visco-analyser respectively. The relationships between parameters measured using these diverse analytical techniques covering a range of length scales are explored using principal component analysis.

2. Materials and methods

2.1. Materials

Starches from seven genotypically distinct barley lines were used in the study along with two wild type (WT) varieties, Golden Promise and Sloop. Three of the test lines were genetically modified using RNAi gene silencing technology to silence the starch biosynthetic enzymes: starch branching enzyme (SBE) IIa (the line ΔSBEIIa), SBE IIb (ΔSBEIIb) and both SBE IIa and SBE IIb (ΔSBEIIa/ΔSBEIIb) (Regina et al., 2010). Each of these gene-silencing steps took place in the variety Golden Promise which is included as an isogenic control for these genotypes. Four other genotypes utilised in the study contain specific gene mutations affecting starch biosynthesis, Waxiro (granule bound starch synthase (GBSS) mutant), *amo1* (high amylose glacier, *amo*1 mutant) and *ssIIa* (starch synthase IIa mutant, *sex6*) and *ssIIa*/*amo1* (double mutant of starch synthase IIa and *amo*1). The starch synthase IIa mutant parent of *ssIIa*/*amo1* line is derived from a sodium azide-treated population of barley variety 'Himalaya' (Morell et al., 2003). The *ssIIa* line is isolated from a back cross of the Himalaya mutant to the barley variety 'Tantangara'.

2.2. Starch extraction

Wholemeal flour from barley samples was soaked in water (1 mL/100 mg flour) for 1 h on a shaker. The soaked flour was spun at 5000 × *g* for 10 min and the supernatant removed. Tris buffer (25 mM, pH 7.5) was added (0.5 mL/100 mg flour), vortexed thoroughly, spun at 5000 × *g* for 5 min and supernatant removed. The pellet was incubated at 37 °C in 2 mL of Tris buffer (25 mM, pH 7.5) and 84 U of proteinase K overnight on a shaker. Following sieving through a nylon mesh, the slurry was spun at 5000 × *g* for 5 min and the supernatant removed. The pellet was washed in 0.05% sodium hydroxide (each time spinning for 5 min at 5000 × *g* and removing the supernatant) followed by two washings with distilled water and three washings with acetone. The starch suspension after the last acetone wash was freeze dried.

2.3. Amylose content (iodometric)

Amylose content based on iodine affinity was estimated as described previously (Regina et al., 2006). Starch (2 mg) was defatted by incubation with 85% methanol at 65 °C followed by dissolving the dried starch in urea-dimethyl sulphoxide (UDMSO) solution (nine parts DMSO and one part of 6 M urea) at a ratio of 1 mL of UDMSO per 2 mg of starch. A 50 μL aliquot of the starch–UDMSO solution was treated with 20 μL of I_2–KI reagent (2 mg iodine, 20 mg potassium iodide per mL of water) and made up to 1 mL volume with water. The absorbance was read at 620 nm. Standard samples containing amylose ranging from 0 to 100%, prepared from potato amylose and corn amylopectin (both from Sigma), were used to generate a standard curve. The absorbance of the test samples was converted to percentage amylose using a regression equation derived from the standard samples.

2.4. Gel permeation chromatography (GPC)

A Sepharose CL-2B column was used to separate and quantify high and low molecular weight fractions from 10 mg of non-debranched starch. The column was equilibrated with 10 mM NaOH and the fractions were eluted at a flow rate of 1 mL min^{-1}. The collected fractions were assayed using a starch content assay kit from Sigma. Apparent amylopectin and amylose contents were estimated as a percentage of the total starch eluting from the column in the first and second peaks, respectively. Pools of the apparent amylose and apparent amylopectin fractions were generated for three starches, Golden Promise, *ssIIa* and ΔSBEIIa/ΔSBEIIb, debranched, and analysed by SE-HPLC.

2.5. Capillary electrophoresis for amylopectin chain length distribution determination using isoamylase and β-amylase

Purified starch (2 mg) was suspended in 750 μL of water in a 2-mL Eppendorf tube by rigorous vortexing followed by the addition of 50 μL of 2 M NaOH. After further vigorous vortexing, to avoid lumps, the solution was boiled for 5 min and allowed to cool at room temperature. Subsequently, 32 μL of glacial acetic acid, 100 μL of 1 M sodium acetate and 1 mL of distilled water were added to the starch solution. Half of the resulting extract was treated with 40 U of isoamylase (from *Pseudomonas* sp., Megazyme) whilst to the other half was added 50 U of β-amylase (from barley, Megazyme). Incubation at 37 °C for 2 h followed in both cases. The solutions were then boiled for 10 min and cooled to room temperature. The β-amylase-treated samples were further treated by isoamylase as indicated above. Isoamylase debranched barley starches were subjected to chain length distribution analysis following the method of O'Shea et al. (O'Shea, Samuel, Konik, & Morell, 1998) using a P/ACE 5510 capillary electrophoresis system (Beckman) with argon-LIF detection. The molar percentage of the chain length distribution represented by chains of 5–12° of polymerisation (DP) and 13–52 DP were calculated and designated in correlation and PCA analyses as "FACE 5-12″ and "FACE 13-52″ respectively. It has

to be noted that reduction in molecular mass due to NaOH or shear induced chain cleavage during starch dissolution or chromatography (see below) has not been specifically quantified in this study.

2.6. Molecular size distribution analysis by size exclusion-high performance liquid chromatography (SE-HPLC)

To 1 mL of isoamylase-treated starch solution, approximately 0.2 g of ion-exchange resin (BioRad AG® 501-X8, Hercules, USA) was added and incubated for 30 min at room temperature while mixing using a rotor. Following incubation, the mixture was spun at 14,000 × *g* for 5 min. The supernatant was filtered through 0.45 μm PVDF filters into HPLC vials. A Waters System configured with a 600 Series Controller, a 717plus autosampler and a 2414 Refractive Index Detector was used for the analysis. A 20 μL aliquot was used for injection. Ammonium acetate buffer (0.05 M; pH 4.7) was used as mobile phase at a flow rate of 0.5 mL min^{-1}. Separation was performed through an Ultrahydrogel™ 250 column (7.8 mm × 300 mm, Waters, Japan) maintained at 60 °C during operation. The column was calibrated for molecular weight using pullulan standards (P800, P400, P200, P100, P50, P20, P10, P5) (Shodex, Kawasaki, Japan). Refractive index measurements were recorded every second. In order to quantify the relative amount of starch eluting in regions of the chromatogram, the total area under the chromatogram was normalised to 100, and that proportion of the refractive index eluting in the following time windows was quantified (Peak 1, 10–11 min; Peak 2, 11–14.5 min; Peak 3, 14.5–16.5 min; Peak 4, 16.5–18.5 min). The proportion eluting between 9.5 and 14.46 min (based on the profile of the low amylose genotype, Waxiro) was accounted as apparent amylose content.

2.7. Solid state ^{13}C nuclear magnetic resonance (NMR) spectroscopy

Solid starch samples were analysed by ^{13}C NMR spectroscopy using the spectral acquisition and interpretation methodology described in Tan, Flanagan, Halley, Whittaker, and Gidley (2007). The solid-state ^{13}C CP/MAS NMR experiments were performed at a ^{13}C frequency of 75.46 MHz on a Bruker MSL-300 spectrometer. Approximately 200–300 mg of starch was packed in a 4 mm diameter, cylindrical, PSZ (partially stabilized zirconium oxide) rotor with a perfluorinated polymer (KelF) end cap. The rotor was spun at 5–6 kHz at the magic angle (54.78°). The 90° pulse width was 5 μs and a contact time of 1 ms was used for all starches with a recycle delay of 3 s. The spectral width was 38 kHz, acquisition time 50 ms, time domain points 2000, transform size 4000, and line broadening 50 Hz. At least 2400 scans were accumulated for each spectrum. Spectra were referenced to external adamantine. The analysis of the NMR spectra involves the decomposition of the spectrum into amorphous and ordered subspectra as described in Tan et al. (2007).

2.8. X-ray diffraction (XRD)

XRD measurements were made with a Panalytical X'Pert Pro diffractometer and as described previously (Blazek, Salman, Rubio, Gilbert, Hanley, & Copeland, 2009). The instrument is equipped with a copper X-ray generator (λ = 1.54 Å), programmable incident beam divergence slit and diffracted beam scatter slit, and an X'celerator high speed detector. X-ray diffraction patterns were acquired at room temperature over the 2θ range of 5°–40° with a step size of 0.0330° 2θ and a count time of 400 s per step.

Assuming a constant divergent slit and a flat-surfaced sample of semi-infinite depth, the experimentally obtained diffraction patterns may be decomposed into a series of distinct diffraction peaks (corresponding to the crystalline phase) and two or three broad amorphous peaks using the modified curve-fitting procedure performed in the Igor software package described by Lopez-Rubio, Flanagan, Gilbert, and Gidley (2008). Crystallinity was calculated as a percentage describing the proportion of the area under the crystalline peaks to the total area; the latter was calculated as the area under the baseline minus the area from background scattering from the instrument and air. The area for background scattering was estimated from the scattering from an empty sample holder. Proportionately, V-type crystallinity was determined as the area under the crystalline peaks at 7°, 13° and 20° 2θ divided by the total area (minus the background area).

2.9. Small-angle X-ray scattering (SAXS)

SAXS measurements were obtained using a Bruker NanoStar SAXS instrument equipped with Vantec 2000 area detector (effective pixel size 54 μm) and pin-hole collimation for point focus geometry and described previously (Blazek et al., 2009). The X-ray source was a copper rotating anode (0.3 mm filament) operating at 45 kV and 110 mA, fitted with cross coupled Göbel mirrors, resulting in a Cu K_α radiation wavelength of 1.5418 Å. The optics and sample chamber were under vacuum to minimize air scattering. Scattering curves are plotted as a function of relative intensity, *I*, versus the magnitude of the scattering vector, *q*: $q = (4\pi/\lambda)\sin\theta$ and where λ is the wavelength and 2θ is the scattering angle. The sample to detector distance was chosen to be 700 mm, which provided a *q*-range from 0.014 to 0.430 $Å^{-1}$. The *q* resolution of the instrument at the main lamellar peak at 0.065 $Å^{-1}$ was calculated to be ca. 0.001 $Å^{-1}$. Samples were presented in 2 mm sealed quartz capillaries as suspensions containing excess water above the sedimented sample and scattering was measured for 60 min. A sealed 2 mm quartz capillary filled with water was used as a background. SAXS datasets were radially averaged using Bruker AXS software 4.1.30. SAXS curves were normalized to sample transmission and background-subtracted using Igor software (Wavemetrics, Lake Oswego, OR, USA). The fitting of the data was carried out using the iterative approach described in the XRD section.

SAXS data were fitted to a power-law function plus Gaussian/Lorentzian peak for the lamellar peak plus Gaussian peak for the second order reflection (Blazek & Gilbert, 2010, 2011):

$$I(q) = k \cdot \frac{I_{01}}{1 + (2(q - q_{01})/B_1)^2} + (1 - k) \cdot I_{01} \exp\left[-\frac{(q - q_{01})^2}{2B_1^2}\right] + I_{02} \exp\left[-\frac{(q - q_{02})^2}{2B_2^2}\right] + Aq^{-\delta} + Bkgd$$

The first and the second term is the Lorentzian and Gaussian component, respectively, that describe the lamellar SAXS peak around 0.065 $Å^{-1}$, where I_0 is the peak height, q_0 is the position of centre of the peak, and *B* is the full width at half maximum of the peak. The third term is a Gaussian peak describing the second order reflection peak around 0.13 $Å^{-1}$. The fourth term is a power-law that describes the scattering arising from structures of larger length-scale than lamellae including interfaces at low *q*, where *A* is the prefactor of the power-law and δ is the exponent of the power-law function. The Bragg spacing *d* was calculated from the position of the peak according to $d = 2\pi/q_0$.

2.10. Differential scanning calorimetry (DSC)

DSC of starch was carried out on a Perkin Elmer Pyris 1 differential scanning calorimeter. Starch and water were pre-mixed at a ratio of 1:2 and approximately 50 mg weighed into a DSC pan which was sealed and left to equilibrate overnight. Measurements were conducted with a heating rate of 10 °C/min from 30 to 130 °C with data being analysed utilising software available with the

instrument. DSC parameters measured were: Gelatinisation Onset Temperature (DSC-Onset), Gelatinisation Peak Temperature (DSC-PT), Gelatinisation End Temperature (DSC-End), Gelatinisation Endotherm (DSC-GE), DSC Amylose/Lipid Endotherm (DSC-AL), Cooling Exotherm (DSC-CE).

2.11. Starch paste viscosity

Starch paste viscosity parameters of barley lines were determined using a Rapid Visco Analyser (RVA, Newport Scientific, Sydney). The temperature profile for the RVA comprised the following stages: hold at 50 °C for 2 min, heat to 95 °C over 6 min, hold at 95 °C for 4 min, cool to 50 °C over 4 min, and hold at 50 °C for 4 min. Thermocline for Windows software was used for collection and analysis of data. Peak viscosity (RVA-PV), viscosity at trough (RVA-T) and final viscosity (RVA-FV) were recorded. Breakdown (RVA-BD; RVA PV minus RVA Trough) and Setback (RVA-SB; RVA FV minus RVA Trough), peak time (RVA-Time) and pasting temperature (RVA-Paste) were calculated using the Thermocline software provided.

2.12. Phosphate content of barley starches

Phosphate groups on the 6′OH of barley starches was assayed by depolymerisation of the starch and enzymatic assay of glucose-6-phosphate content. This method does not measure the total phosphate content of starch as phosphate attached to the 3′OH is not measured. Glucose-6-phosphate was estimated by an adapted amyloglucosidase assay using the starch assay kit from Roche (Germany). Barley starch (20 mg) was pre-digested at 90 °C for 15 min using 30 units of Thermostable alpha-amylase 3000 unit mL^{-1} (Megazyme) followed by centrifuging for 15 min at 10,000 rpm. Amyloglucosidase assay was preformed on the supernatant using 5 μL of glucose-6-phosphate dehydrogenase (270 units mg^{-1} protein, from Sigma) specifically instead of the kit solution containing hexokinase and glucose-6-phosphate dehydrogenase. The amount of glucose-6-phosphate was reported as proportion of the total amount of digested starch present in the sample measured by using the starch assay kit from Roche.

2.13. Resistant starch content

The resistant starch content of the barley starch granule preparations was determined using an in vitro method quantitatively validated using in vivo data from human ileostomates studies (Bird, Usher, May Topping, & Morell, 2012).

2.14. Statistical analysis

Correlation and principal component analysis (PCA) of starch parameters was carried out using the "cor" and "prcomp" functions in the statistical software package R (R Development Core Team, 2009). The PCA analysis was based on the correlation matrix and traits were scaled (Team, 2009).

3. Results

3.1. Variation in amylose content

Three independent methods, iodine affinity of defatted starch (IA), gel permeation chromatography of non-debranched starch (GPC) (Fig. 1) and size exclusion-high performance liquid (SE-HPLC) chromatography of isoamylase debranched starch (SEC), were used to measure the apparent amylose contents of the nine barley genotypes included in this study (Table 1). The apparent amylose values generated by the three methods were highly correlated (see Supplementary Table 3), however, the absolute apparent amylose values generated by each method differed substantially, with debranched SE-HPLC giving the lowest values, the iodometric method giving intermediate values, and the undebranched GPC method giving the highest values ($r^2 = 0.88$). The amylose contents of *amo1* was elevated above wild type levels (IA: 39.1%; SEC 29%, GPC 49.4%). The genotypes *ssIIa*, *ssIIa*/*amo1*, ΔSBEIIa and ΔSBEIIa/ΔSBEIIb contained genetic modifications resulting in further elevation of amylose content. ΔSBEIIa/ΔSBEIIb gave the highest amylose content (IA, 69.4%, SEC 38.7%, GPC 86.0%).

3.2. λ_{max} of amylose and amylopectin fractions

The λ_{max} value of starch is known to increase with the presence of chains/branches of higher degree of polymerisation (Bailey & Whelan, 1961; Yasui, Ashida, & Sasaki, 2009) and, therefore, λ_{max} values were determined for both amylopectin and amylose fractions (from all nine barley starches) following elution from gel permeation chromatography (Table 1). The λ_{max} of the GPC fraction containing the highest level of amylopectin was determined for each of the genotypes analysed with values ranging from 510 nm in Waxiro to 550 nm in ΔSBEIIa/ΔSBEIIb and ΔSBEIIa (Table 1). The amylopectin λ_{max} values correlate with the apparent amylose content by iodine affinity ($r^2 = 0.74$) and GPC ($r^2 = 0.59$); however, it was noted that there were two samples that were not highly correlated – the *amo1* starch which had a λ_{max} more typical of a wild type starch than a high amylose starch, and ΔSBEIIa, which had a λ_{max} value that was higher than expected given its intermediate amylose content (data not shown). Demonstrating that these samples have anomalous starches, removal of these samples from the correlation analysis gave r^2 values of 0.92 and 0.915 for the remaining 7 samples with apparent amylose determined by iodine affinity and GPC respectively. The λ_{max} of amylose ranged from 570 nm in Waxiro to 615 nm in *ssIIa*/*amo1*. While starches from genotypes with SBE IIa mutation had a lower λ_{max} value for amylose, those with ssIIa and amo1 mutations resulted in higher λ_{max} value compared to the wild type suggesting the possibility of ssIIa and amo1 mutations resulting in amylose with longer chain lengths compared to SBE IIa mutations. Further investigation is required to confirm this possibility.

3.3. Molecular size distribution of debranched barley starches

Molecular structure of amylose and amylopectin was further investigated by SE-HPLC following isoamylase debranching. The profiles for various barley genotypes are given in Fig. 2 and starch contents in 4 regions of the profile (Peak 1, Peak 2, Peak 3, and Peak 4) are given in Table 2. The two wild type starches used in the study, Sloop and Golden Promise, had essentially similar profiles with two clear peaks, a higher molecular weight fraction eluting between 11 and 14.5 min (designated Peak 2) and a second lower molecular weight fraction eluting between 16.5 and 18.5 min (designated Peak 4). The profile of the starch from Waxiro showed that this starch was predominantly composed of low molecular weight material in Peak 4 with a very low level of high molecular weight chains in Peak 2, consistent with the majority of the Peak 2 material being derived from amylose and Peak 4 from amylopectin. A shoulder peak (Peak 3) was observed for all starches ahead of the Peak 4 between 14.5 and 16.5 min, and was most pronounced in starches with down-regulated branching enzyme contents (ΔSBEIIa, ΔSBEIIb, or ΔSBEIIa/ΔSBEIIb). The Peak 4 region for genotypes with ssIIa mutations (*ssIIa* and *ssIIa*/*amo1*) shows a pronounced double peak eluting between 16.5 and 18 min in contrast to the other starch genotypes examined in the study. The high amylose starches (ΔSBEIIa/ΔSBEIIb, ΔSBEIIa, *ssIIa* and

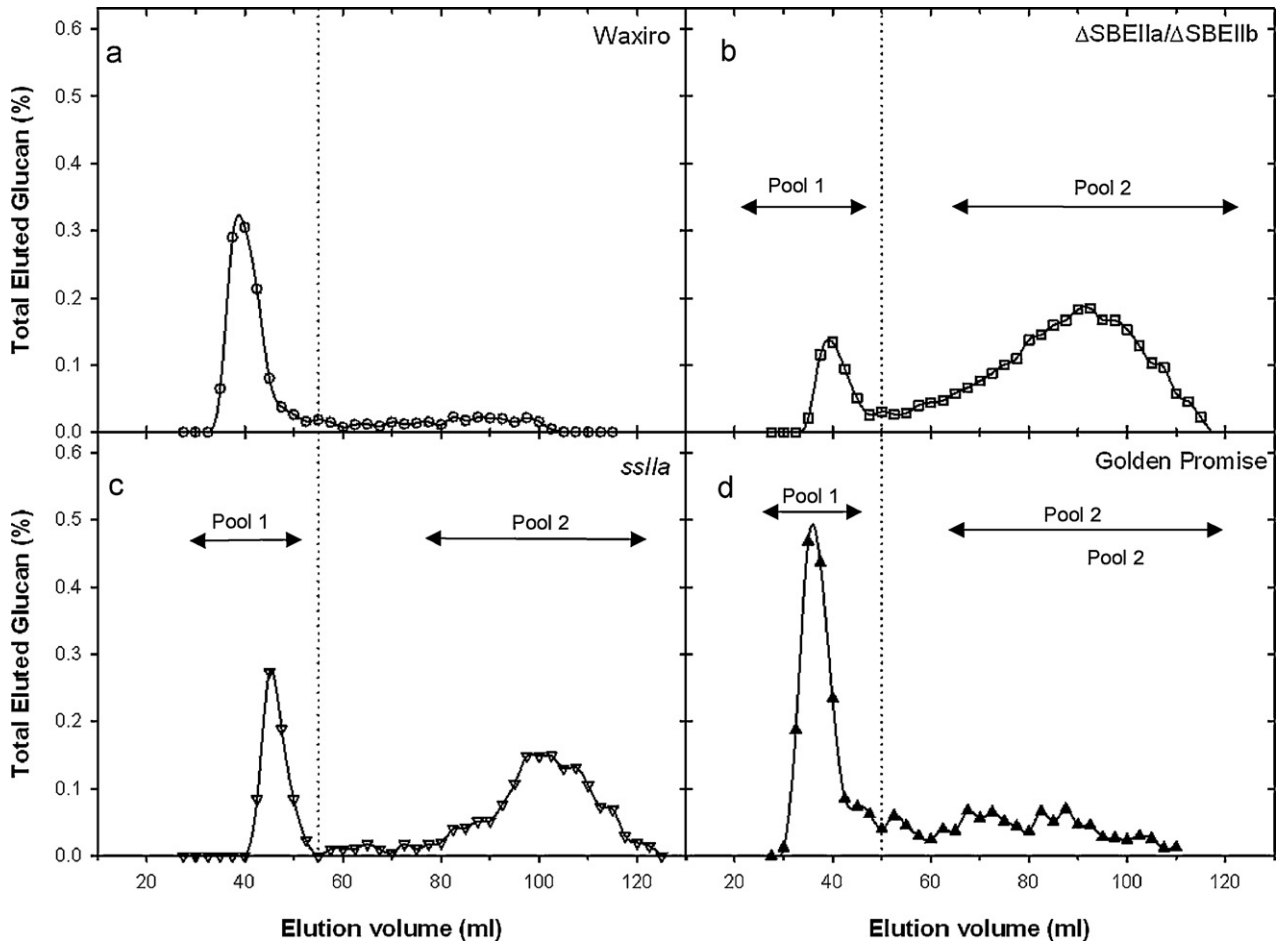

Fig. 1. Sepharose CL-2B Gel permeation chromatography analysis of starch from four barley genotypes; (a) Waxiro, (b), ΔSBEIIa/ΔSBEIIb, (c) *ssIIa*. (d) Golden Promise – the percentage of the total starch eluting from the column in the first and second peaks are estimated as apparent amylopectin and amylose respectively. The vertical dotted line indicates demarcation of the regions under amylopectin and amylose peaks. Pools of fractions applied to SEC analysis (see Fig. 3) are as marked.

ssIIa/*amo1*) contained an additional high molecular weight peak eluting between 10 and 11 min, designated Peak 1.

To further characterise the amylose and amylopectin from high amylose starches, pooled fractions of these two undebranched components separated through GPC (pooled as shown in Fig. 1) from two high amylose lines ΔSBEIIa/ΔSBEIIb and *ssIIa* and a control line Golden Promise were subjected to SEC following isoamylase debranching. Five to six fractions between the high molecular weight (Pool 1) and low molecular weight (Pool 2) peaks were discarded in order to clearly separate the two fractions. Fig. 3b shows the profiles of Pool 2 from the three genotypes. The debranched SE-HPLC profile of Pool 2 material from ΔSBEIIa/ΔSBEIIb is consistent with the presence of all 4 peaks seen in the debranching of total starch (Peak 1, Peak 2, Peak 3 and Peak 4) being present in Pool 2 material. In contrast, Pool 1 contains only products expected of amylopectin debranching, Peak 3 and Peak 4, with minimal contamination from Peak 2 and no detectable Peak 1 present (Fig. 3a).

3.4. Phosphate content of barley starches

The 6′OH phosphate content of the barley starches was determined after depolymerisation and the resultant glucose-6-phosphate/total glucan (G6P/G) ratio is given in Table 2. No strong

Table 1
Amylose contents and λ_{max} of amylopectin of barley genotypes.

Genotype Data label	Apparent amylose content (%) by iodine blue value[a] AM-Iodine	Apparent amylose content (%) by sepharose CL-2B GPC AM-GPC	Apparent amylose content (%) by SE-HPLC AM-SEC	λ_{max} of amylopectin (nm) AP-λ_{max}
Waxiro	5.0 ± 0	14.3	2.6	510
Sloop	30.0 ± 0.1	36.1	17.3	530
Golden Promise	31.4 ± 1.0	32.2	21.6	520
amo1	39.1 ± 1.3	49.4	29.0	515
ssIIa	50.7 ± 1.0	69.9	30.5	540
ssIIa/amo1	60.6 ± 2.0	64.9	36.8	540
ΔSBEIIb	33.9 ± 0.7	33.7	21.3	530
ΔSBEIIa	53.6 ± 0.2	50.6	31.7	550
ΔSBEIIa/ΔSBEIIb	69.4 ± 1.1	86.0	38.7	550

[a] Mean of three replicates.

Table 2
Starch structural and functional parameters of barley genotypes.

Data label	Proportions of starch eluting from SE-HPLC of debranched starches (fractions defined in Section 2)				Glucose-6-P to glucose ratio[a] ($\times 10^{-4}$)	Resistant starch content[a] (g RS/g starch) %
	Peak 1	Peak 2	Peak 3	Peak 4	G6P	RS
Waxiro	0.1	4.0	17.5	78.5	2.43	0.1
Sloop	0.7	23.3	14.0	61.9	2.24	0.6
Golden Promise	1.2	23.4	14.1	61.3	2.72	0.2
amo1	1.6	31.6	12.0	54.9	2.37	0.9
ssIIa	5.5	39.3	12.1	43.1	2.89	1.9
ssIIa/amo1	4.3	33.7	14.1	47.9	3.20	3.4
ΔSBEIIb	1.3	24.3	17.1	57.3	3.78	0.2
ΔSBEIIa	6.6	29.5	19.6	44.3	5.28	0.9
ΔSBEIIa/ΔSBEIIb	7.3	33.4	23.5	35.8	2.26	6.3

[a] Mean of three replicates.

correlation of G6P/G ratio with amylose content was observed, with a *R*-value of 0.247 or lower for all three amylose content estimation methods (see Supplementary Table 3). The highest G6P/G ratio was observed in ΔSBEIIa, an elevated amylose line, and the lowest value in Sloop (normal amylose line) and ΔSBEIIa/ΔSBEIIb (highest amylose line).

3.5. Chain length distribution of debranched barley starches

Chain length distribution of isoamylase debranched starch was analysed by fluorophore assisted carbohydrate electrophoresis (FACE). The normalised molar chain length distribution of Golden Promise starch was subtracted from that of each of the starches and presented as a difference plot in Fig. 4. The Waxiro, Sloop and ΔSBEIIb starches showed only minor differences (<0.5%) from the Golden Promise control. The debranched *amo1* starch showed a greater degree of difference, with an increased proportion of chains of DP 11–29 and a decreased proportion of DP 6–9 (Fig. 4c). A less severe reduction in the proportion of chains of DP ≥ 37 was also observed in this starch. The changes observed in the chain length distribution largely agreed with previous studies on *amo1* starches (Bertoft, Kallman, Koch, Andersson, & Aman, 2011;

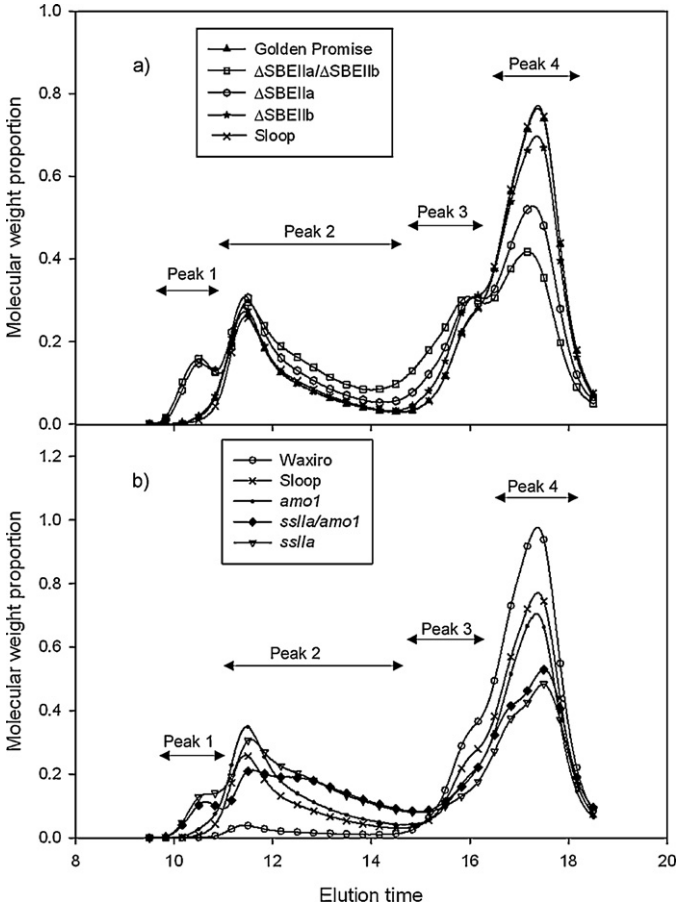

Fig. 2. Molecular weight distribution analysis of isoamylase debranched barley starches by size exclusion-high performance liquid chromatography (SE-HPLC). Genotypes are indicated in panels (a) and (b) respectively. The peaks are designated according to the order of elution as Peaks 1, 2, 3 and 4. The major high molecular weight elution peak is designated as Peak 2 and the major low molecular weight elution peak is designated as Peak 4.

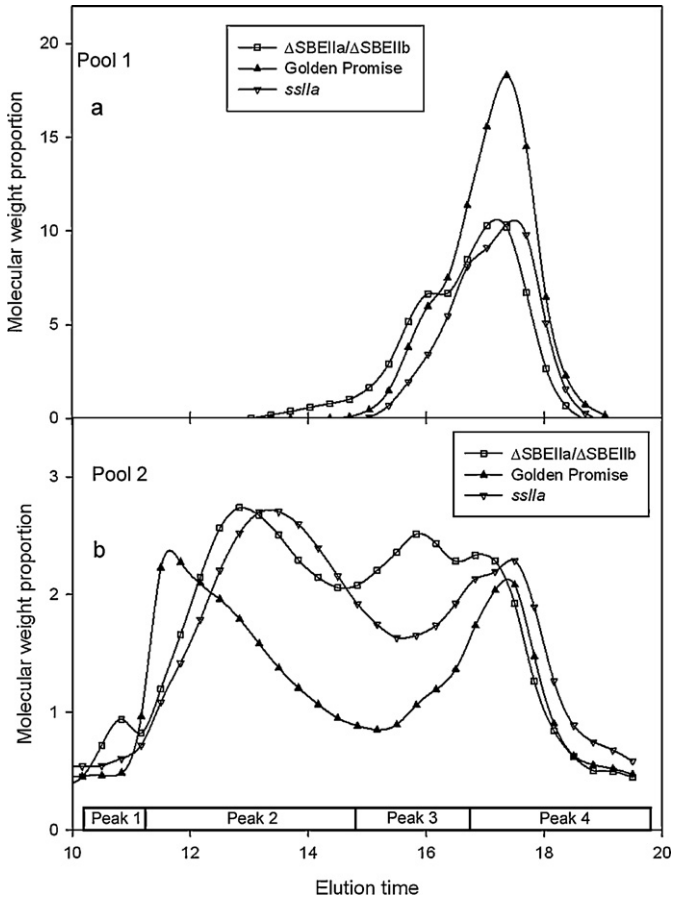

Fig. 3. Analysis of isoamylase debranched molecular weight distribution of starch pools generated by gel permeation chromatography of three barley starch genotypes. High molecular weight (Pool 1) and low molecular weight (Pool 2) fractions were generated as described in Fig. 1 and separated by SE-HPLC. Genotypes are indicated in panels (a) and (b) respectively. The region under various peaks are defined according to the elution time windows defined in Fig. 2.

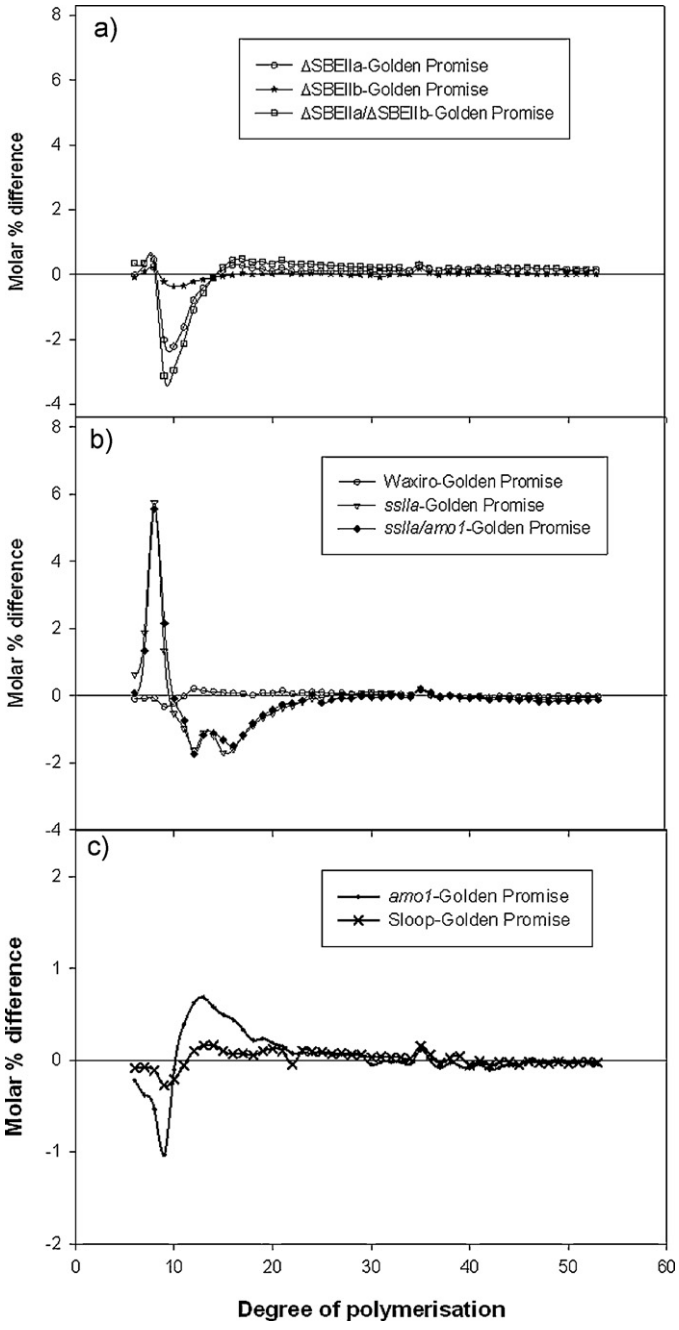

Fig. 4. FACE analysis of isoamylase debranched starches. Chain length distribution was obtained through capillary electrophoresis of APTS labelled glucan following isoamylase debranching of starch. The chain length distribution for Golden Promise has been subtracted from each genotype to generate a difference plot. Genotypes are as indicated in panels (a), (b) and (c) respectively.

Matsuki, Yasui, Sasaki, Fujita, & Kitarnura, 2008). Consistent with previous studies major and opposite effects were observed for the lines with either SBEIIa or SSIIa down-regulation. In ΔSBEIIa and ΔSBEIIa/ΔSBEIIb, starches, a significant reduction in DP 9–13 was observed, while there is an increase in the proportion of chains of DP 6–8 and DP > 15 (Fig. 4a). These changes were more marked for the ΔSBEIIa/ΔSBEIIb starch compared to the starch from ΔSBEIIa. In contrast, the high amylose starches *ssIIa* and *ssIIa/amo1*, exhibited an entirely different chain length profile with a significant increase in the proportion of DP 6–9 and a reduction in the DP 11–24 (Fig. 4b). Within the DP range of 11–24, a bimodal distribution in relation to Golden Promise was observed in both *ssIIa* and *ssIIa/amo1*.

3.6. Chain length distribution of β-limit dextrin

The internal branching pattern of starch was further studied through analysis of the chain length distribution profile of the β-limit dextrin generated by β-amylolysis, followed by isoamylase debranching and chain length analysis using FACE. Normalised FACE profiles of β-limit dextrin from the various starches are provided in Supplementary Fig. 1. Previous work has suggested the designation of four classes of chains in the debranched amylopectin profile, classified as B1a (6–8 DP), B1b (9–21 DP), B2 (22–50 DP) and B3 (>50 DP) consistent with previous groupings from limit dextrins (Bertoft, 2004; Yao, Thompson, & Guiltinan, 2004). Two features were observed from this analysis. Firstly, the starches from *amo1*, ΔSBEIIa and ΔSBEIIa/ΔSBEIIb show an increase in chain length in the DP 7–9 range compared to the other lines. Secondly, the ΔSBEIIa and ΔSBEIIa/ΔSBEIIb lines show a pronounced peak from DP 21–31. A small peak is also present in the *ssIIa* and *ssIIa*/*amo*1 high amylose starches but is much less pronounced. Differences in the very short chains of DP 2–6 are not studied in this paper due to poor reproducibility of data derived from this region using the FACE system used.

3.7. Crystallinity of barley starch granules

Previous studies reported that normal barley cultivars display the typical A-type crystalline diffraction pattern of cereal starches with a main diffraction doublet at 17° and 18° 2θ and peaks at 15°, 20° and 23° 2θ (Lopez-Rubio et al., 2008; Waduge, Hoover, Vasanthan, Gao, & Li, 2006). Consistent with the literature, wild barley cultivars Golden Promise and Sloop exhibited A-type crystalline patterns with 18–19% crystallinity including 3% corresponding to V-type reflections (Table 3). It must be noted that the proportion of V-type crystallinity was calculated based on the area under the peaks around 7°, 13° and 20° 2θ and may over-estimate the actual proportion of single helical amylose crystals due to overlapping peaks corresponding to A or B-type crystal structures. Waxiro exhibited the highest crystallinity among the cultivars studied of 30% with well-defined diffraction peaks at positions characteristic for A-type crystallinity and insignificant V-type reflections (Table 3, Supplementary Fig. 2). The genotypes with intermediate amylose content, ΔSBEIIa and *amo1* showed crystalline type and quantity similar to the lower amylose cultivars (18% total including 3% V-type crystallinity). It is noteworthy that unlike the other elevated amylose starches investigated in this study, the SBEIIa starch retains an A-type crystallinity.

In contrast, the high-amylose lines ΔSBEIIa/ΔSBEIIb, *ssIIa* and *ssIIa/amo1* produced a B-type pattern with differing proportions of V-type crystalline peaks (Supplementary Fig. 2b). B-type crystallinity is characterized by a main diffraction peak at 16.9° 2θ and peaks at 5.5°, 14.6°, 22.3° and 23.7° 2θ (Lopez-Rubio et al., 2008). ΔSBEIIa/ΔSBEIIb had 15% crystallinity including 4% corresponding to V-type crystals (Table 3, Supplementary Fig. 2a) whereas *ssIIa* displayed mixed 'B + V' crystallinity of 16% (with 8% V-type crystallinity) and *ssIIa/amo1* contained a lower quantity of V-type crystals (5%). Starches from amylose extender (ae) mutant rice and maize in which SBE IIb is defective demonstrated a B-type crystallinity; this is in contrast to SBE IIb reduced barley that failed to show ae phenotype, and the starch of which retained the A-type crystallinity (Kubo, Yuguchi, Takemasa, Suzuki, Satoh, & Kitamura, 2008; Li, Guiltinan, & Thompson, 2007; Li, Jiang, Campbell, Blanco, & Jane, 2008). The effect of *ssIIa* mutation on crystallinity in barley is also different to that in maize where the sugary 2 mutant starch retained the A-type crystallinity (Campbell, White, & Pollak, 1994) whereas in barley the crystallinity is modified to the B + V form (Morell et al., 2003). A recent X-ray diffraction study on six hull less barley starches with amylose contents ranging from 1.3%

Table 3
Parameters from fitting of XRD, SAXS and ^{13}C CP/MAS NMR data from samples used in this study.

Data label	X-ray diffraction			Small-angle X-ray scattering				^{13}CP/MAS NMR	
	Crystalline pattern[a]	Total crystallinity[a] (%) XRD-Total	V-type crystallinity[a] (%) XRD-V	Lamellar peak intensity[b,c] SAX-LPI	Lamellar peak position[b,c] ($Å^{-1}$) ($\times 10^{-2}$) SAX-LPP	Width of the lamellar peak[b,c] ($\times 10^{-2}$) SAX-WLP	Lamellar repeat distance (nm)[b] SAX-LRD	Double helices (%) NMR-DH	Amorphous starch (%) NMR-AS
Waxiro	A	29.7	0.0	12160 (10)	6.02 (9)	2.35 (9)	10.4	31	65
Sloop	A	19.3	2.6	6256 (9)	6.03 (2)	2.77 (1)	10.4	32	62
Golden Promise	A	18.2	2.7	6460 (20)	6.03 (2)	2.42 (3)	10.4	33	61
amo1	A	18.3	2.7	4280 (10)	5.47 (3)	2.76 (2)	11.5	25	71
sslla	B + V	16.3	7.7	3380 (10)	4.57 (7)	4.14 (9)	13.7	5	91
sslla/amo1	B + V	15.5	5.2	6590 (20)	3.26 (8)	3.75 (7)	19.3	10	89
ΔSBEIIb	A	18.1	2.7	5145 (9)	6.25 (2)	2.91 (1)	10.1	31	65
ΔSBEIIa	A	18.2	2.7	4800 (10)	6.17 (2)	2.69 (2)	10.2	28	66
ΔSBEIIa/ΔSBEIIb	B + V	14.6	4.0	2330 (8)	5.04 (8)	3.85 (1)	12.5	24	72

[a] Crystallinity was calculated from the XRD data by peak-fitting procedure described in the text.
[b] SAXS peak fitting parameters represent best fits of single power-law function plus Gaussian-Lorentzian function to the lamellar peak and a single Gaussian peak to a second reflection peak. Q-resolution is 0.001 for SAXS.
[c] The number in brackets correspond to uncertainty in fitting parameter.

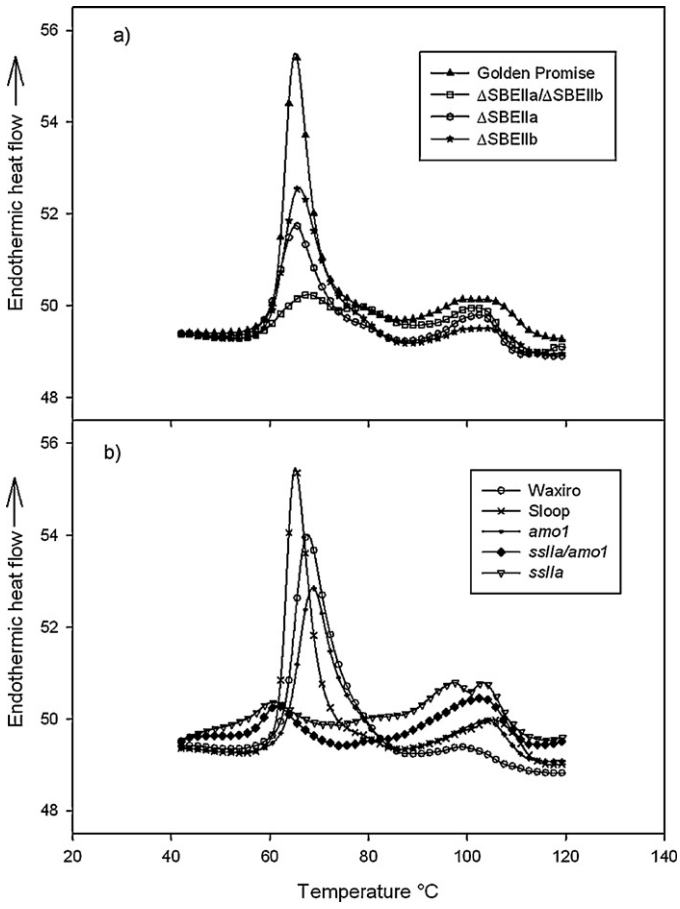

Fig. 5. Differential scanning calorimetry (DSC) analysis of nine barley genotypes as shown in panel (a) and (b).

to 35.4% revealed an A-type diffraction pattern in all six starches (Gao, Vasanthan, & Hoover, 2009).

3.8. Small-angle X-ray scattering from barley starch granules

SAXS curves were characterised by intense scattering at low q, which rapidly decreased at larger angles and featured three scattering peaks: a lamellar peak at $q \approx 0.06$–$0.07\ Å^{-1}$, a broad second order reflection peak at 0.12–0.13 $Å^{-1}$ and a peak at 0.4 $Å^{-1}$ corresponding to the interhelix distance between the 100 crystallographic planes in the hexagonal unit cell of B-crystalline starch. A comparison of the SAXS is shown in Fig. 5 highlighting variations around the principal lamellar peak. All SAXS data were fitted to a single power-law function plus a combined Gaussian–Lorentzian function (for the lamellar peak) and a further Gaussian function to describe the higher order lamellar reflection at 0.12–0.13 $Å^{-1}$. Fitting parameters are shown in Table 3. The intensity of the lamellar peak ranged from 2300 r.u. (relative intensity units) for ΔSBEIIa/ΔSBEIIb starch to 12,164 r.u. for Waxiro (Table 3, Supplementary Fig. 3) and the repeat distance ranged from 10.1 to 19.3 nm.

Waxiro showed the most defined lamellar peak with an intensity of ca 12,000 r.u. centred at 0.060 $Å^{-1}$, which corresponds to lamellar repeat distance of 10.4 nm (Supplementary Fig. 3a). The control barley cultivars Golden Promise and Sloop displayed a lamellar peak which was less defined (intensity of ca. 6000 r.u.) but with the same peak centre as Waxiro. The genotypes ΔSBEIIa and ΔSBEIIb displayed more reduced lamellar peak intensity (4800 and 5100 r.u., respectively) with peak centre shifted to higher q, corresponding to shorter lamellar repeat distances (10.2 and 10.1,

respectively). The intermediate amylose content genotype *amo1* showed a lamellar peak intensity of ca. 4300 r.u. and lamellar repeat distance of 11.5 nm.

The high-amylose genotypes ΔSBEIIa/ΔSBEIIb, *ssIIa* and *ssIIa/amo1* exhibited different scattering curves to the remaining genotypes (Supplementary Fig. 3b). The lamellar peak was much broader, much less intense and shifted to lower *q*. Fitting parameters as shown in Table 3 indicate that the lamellar repeat distance is larger for these three cultivars with ΔSBEIIa/ΔSBEIIb having a mean distance of 12.5 nm, *ssIIa* 13.7 nm and *ssIIa/amo1* 19.3 nm. The extremely poorly defined peaks for these cultivars are likely to indicate a severely disrupted and/or non-existent lamellar structure compared to normal and waxy cultivars.

3.9. Solid state ^{13}C CP/MAS NMR of barley starches

Solid state ^{13}C CP/MAS NMR detects short range molecular order and provides a measure of the helix content in starch granules. Subtraction of amorphous spectral features (Tan et al., 2007) from the spectra of nine barley starches revealed the C-1 (94–105 ppm) triplet signal characteristic of the A-type double helical conformation in all the starches except *ssIIa*, *ssIIa/amo1* and ΔSBEIIa/ΔSBEIIb (Supplementary Fig. 4). In these three starches the C1-signal indicated the presence of both B-type (doublet) and V-type (singlet) polymorphs. Thus the NMR method was able to correctly assign crystalline polymorphs independent of XRD data. The estimated values of the relative proportions of the amorphous and double helical conformations for the barley starches are summarized in Table 3. The *ssIIa* and *ssIIa/amo1* starches had a significantly lower proportion of double helices followed by *amo1* and ΔSBEIIa/ΔSBEIIb compared to all other starches. The percentage of amorphous polymorph was also higher in these starches, with extreme values in *ssIIa* and *ssIIa/amo1* compared to all other starches. The estimated value for V-type polymorph was 6% or less for all lines (data not shown).

3.10. DSC parameters of barley starch gelatinisation

The thermal behaviour of various barley starches in excess water was studied using DSC (Fig. 5, Supplementary Table 1). The control genotypes used in this study gave very similar values for gelatinisation onset, peak and final temperatures, and gelatinisation enthalpy (ΔH) values. Consistent with previous findings (Matsuki et al., 2008), the *amo1* and Waxiro starches had higher values of onset, peak and end of gelatinisation temperatures compared to both the controls (Golden Promise and Sloop), however, while Waxiro showed an increased ΔH value compared to the control genotypes, the ΔH value decreased for the *amo1* starch. Small differences in gelatinisation onset, peak and end temperatures were observed for ΔSBEIIa and ΔSBEIIb, and both starches had decreased ΔH values compared to the controls. In general, the three highest amylose starches, ΔSBEIIa/ΔSBEIIb (Fig. 5a), *ssIIa* and *ssIIa/amo1* (Fig. 5b) gave a broad DSC profile compared to other starches. These three starches had striking decreases in ΔH values to 0.35 ± 0.08, 0.47 ± 0.15 and 1.11 ± 0.09 respectively, however, they differed in the impact on gelatinisation temperature profiles. Gelatinisation onset temperature decreased for all three high amylose starches, but whereas the *ssIIa* and *ssIIa/amo1* starches showed decreased peak and final gelatinisation temperatures, ΔSBEIIa/ΔSBEIIb gave a broad gelatinisation profile with significantly increased peak and final gelatinisation temperatures.

The reversible high temperature transition revealed by DSC in starches well above the gelatinisation endotherm (Fig. 5) has been assigned to melting of the amylose–lipid complex (Biliaderis, Page, Slade, & Sirett, 1985). Amylose/lipid dissociation endotherms fell outside the range of the control genotypes for only three samples (Supplementary Table 1). The low amylose/lipid endotherm for Waxiro (0.34 J/g) is consistent with the low lipid content of waxy starches (Morrison, Law, et al., 1993; Morrison, Tester, et al., 1993). Amylose/lipid dissociation enthalpies for *ssIIa* (2.39 J/g) and *ssIIa/amo1* (1.44 J/g) are higher than the control varieties. All starches studied except Waxiro exhibited a reversible melting transition exotherm also with a peak recorded between 85 °C and 95 °C (data not shown). The starches from *ssIIa* and *amo1/ssIIa* exhibited a higher value for cooling exotherm enthalpy compared to all other starches (Supplementary Table 1).

3.11. RVA pasting properties of barley starches

Starches from the nine barley genotypes displayed wide diversity in pasting properties determined by RVA. The peak viscosity ranged from 9.1 RVU in *ssIIa* starch to 420 RVU in ΔSBEIIb starch (Supplementary Table 2). The final viscosity was also highest (438 RVU) in ΔSBEIIb starch. Starch from ΔSBEIIa/ΔSBEIIb recorded the lowest final viscosity value of 13.2 RVU closely followed by *ssIIa/amo1* (16.4 RVU).

3.12. Resistant starch (RS) content

The resistant starch content of the extracted barley starches was determined using a validated in vitro method that simulated the major stages of carbohydrate digestion in the human upper gastrointestinal tract (Table 2). The RS value ranged from 6.3% in ΔSBEIIa/ΔSBEIIb to 0.1% in Waxiro. Resistant starch values obtained were highly correlated with amylose content (Supplementary Table 3).

3.13. Principal component analysis (PCA)

The relationship between genotypes and starch molecular structure as well as functionality was elucidated by carrying out PCA. The first three principal components (PC), PC1, PC2 and PC3 accounted for more than 85% of the variance. The relationships between traits and genotypes are shown in plots of PC1 against PC2 (Fig. 6), PC1 against PC3 (Supplementary Fig. 5), PC2 against PC3 (Supplementary Fig. 6) and the correlation coefficients are given in Supplementary Table 3.

4. Discussion

The availability of a unique collection of defined barley genotypes ranging in amylose content from 5 to 69% (by iodometric analysis) provided the opportunity for a comprehensive analysis of the relationships between starch structure and functionality. This paper builds on previous studies (Morell et al., 2003; Regina et al., 2010; Schondelmaier et al., 1992) extending both the range of genotypes analysed and through the utilisation of a wide range of analytical techniques to analyse starch properties at the molecular (amylose content by iodine affinity and GPC of non-debranched starch, SEC of isoamylase debranched starch, FACE analysis of debranched starch and the debranched β-limit dextrin, 6′OH phosphate content), granular (XRD, solid state NMR and SAXS) and functional (DSC, RVA and resistant starch)) levels. The barley genotypes utilised in this study have resulted from mutations (Waxiro, *amo1*, *ssIIa*, *ssIIa/amo1*) or the use of RNAi technology to down-regulate specific genes (ΔSBEIIa, ΔSBEIIb, ΔSBEIIa/ΔSBEIIb).

To investigate the relationships between the diverse traits measured within the various barley genotypes used, principal components analysis (PCA) was conducted. Principal components (PC) 1–6 accounted for 98.9% of the variance with PC1, PC2 and PC3 accounting for 56%, 18% and 12.5% of the variance respectively. In the plot of PC1 against PC2 (Fig. 6), the distribution of genotypes

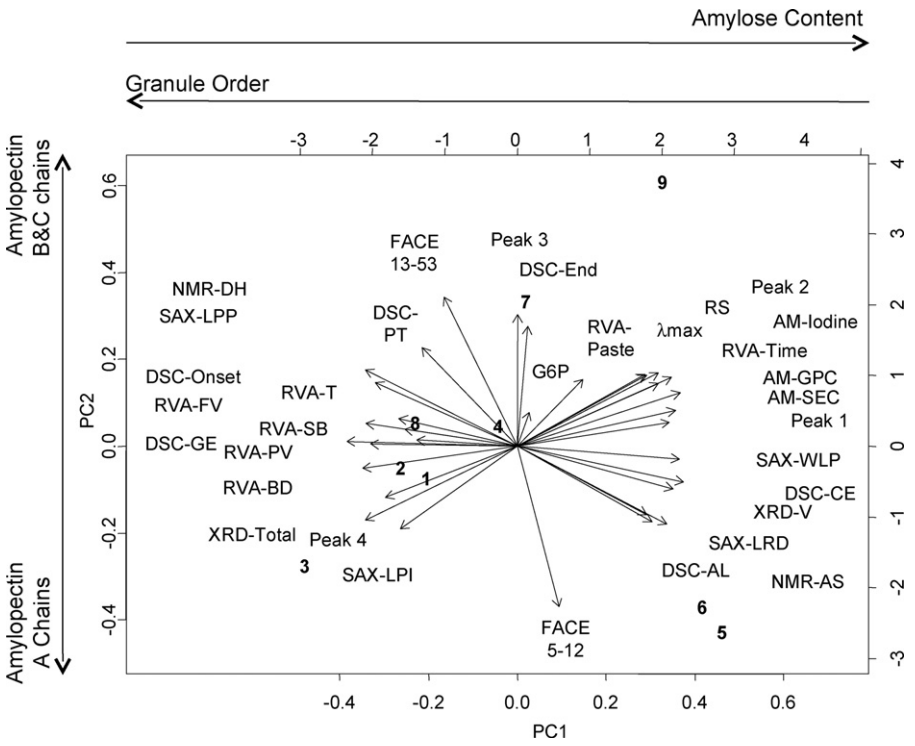

Fig. 6. Principal components analysis of barley starches. Loadings for the first two principal components (PC1 and PC2) plotted against each other. Abbreviations for the various parameters are defined in Table 4. Numbers refer to genotypes as follows: 1; Sloop; 2; Golden Promise; 3; Waxiro; 4; *Amo1*; 5; *ssIIa*; 6; *ssIIa/amo1*; 7; ΔSBEIIa; 8; ΔSBEIIb; 9; ΔSBEIIa/ΔSBEIIb.

Table 4
Parameters associated with principal components 1, 2 and 3.

Granule order		Granule disorder	
Structural	Functional	Structural	Functional
Principal component 1			
Peak 4	DSC onset temperature (DSC onset)	Amylose content determined by gel permeation chromatography of undebranched starch (AM-GPC)	Resistant starch (RS)
SAXS lamellar peak position (SAX-LPP)	DSC gelatinisation endotherm (DSC-GE)	Amylose content determined by size exclusion chromatography of isoamylase debranched starch (AM-SEC)	DSC cooling exotherm (DSC-CE)
SAXS lamellar peak intensity (SAX-LPI)	RVA peak viscosity (RVA-PV)	Amylose content determined by iodine affinity measurement (AM-Iodine)	RVA peak time (RVA–time)
NMR double helices (NMR-DH)	RVA breakdown (RVA-BD)	AP-λ_{max}	DSC amylose/lipid endotherm (DSC-AL)
XRD total crystallinity (XRD-Total)		Peak 2 Peak 1 XRD V-type crystallinity (XRD-V) NMR amorphous starch (NMR-AS) SAX lamellar repeat distance (SAX-LRD) SAX width of the lamellar peak (SAX-WLP)	

Amylopectin A chains		Amylopectin B & C chains	
Structural	Functional	Structural	Functional
Principal component 2			
FACE 5-12		FACE 13–53 Peak 3 DSC End Temperature (DSC-End)	DSC peak temperature (DSC-PT)

Structural	Functional	Structural	Functional
Principal component 3			
		G6P to glucose ratio (G6P)	RVA paste temperature (RVA-Paste) RVA setback (RVA-SB) RVA final viscosity (RVA-FV) RVA trough (RVA-T)

across PC1 (the *x*-axis) suggests that PC1 is significantly influenced by starch granule order parameters (Table 4), given that different genotypes of barley lines are distributed from starches with high degrees of starch granule order (Waxiro, Sloop, Golden Promise and ΔSBEIIb genotypes) at low PC1 values, through the genotypes with intermediate starch granule order (*amo1* and ΔSBEIIa) to low starch granular order genotypes (ΔSBEIIa/ΔSBEIIb, *ssIIa* and *ssIIa/amo1*). Table 4 provides a list of starch structural and functional parameters that were aligned with PC1 in both the PC1 × PC2 plot and PC1 × PC3 plot. The dominant structural feature aligning with PC1 is the relative content of amylopectin and amylose.

PC2 separates the barley genotypes on an independent basis to PC1, with *ssIIa* and *ssIIa/amo1* at one end of the spectrum and ΔSBEIIa/ΔSBEIIb at the other (Fig. 6, Supplementary Fig. 5). Structural features of starch aligning with PC2 and the distribution of genotypes are amylopectin debranched chain length parameters (Table 4). Several lines of evidence from this study demonstrate that factors determining amylopectin chain length distribution are independent to the amylose content of starch. Firstly, the opposite impacts on amylopectin chain length distribution of the *ssIIa* and *ssIIa/amo1* group compared to the ΔSBEIIa plus ΔSBEIIa/ΔSBEIIb group. Secondly, within this latter group, ΔSBEIIa/ΔSBEIIb has a very high amylose content whereas ΔSBEIIa, while having an almost comparable impact on amylopectin chain length distribution, has substantially lower amylose content. Furthermore, the starch of the SBEIIa genotype is characterised by having an A-type crystalline form, which is unusual for a starch with elevated amylose content and a debranched amylopectin chain length distribution containing an increased proportion of longer chain lengths. It is unclear whether the properties of the starch per se determine the crystalline packing arrangement for starches or whether packing form is determined during synthesis by the enzyme machinery synthesising the amylopectin molecular structure. This is a subject for further research. PC3 accounts for only a small percentage of the variance. While PC3 aligns with various RVA functional parameters, the only structural feature to align with PC3 is the G6P/G ratio (Table 4, Supplementary Fig. 6).

As has been observed previously (Blazek et al., 2009), waxy genotypes, such as the Waxiro line included in this study, are associated with high total crystallinity and lamellar peak intensity as determined by SAXS. The control lines Golden Promise and Sloop are characterised by an ordered granular structure at wild type amylose levels (30.0–33.9% amylose by iodometric analysis) although neither total crystallinity nor lamellar peak intensity are pronounced as seen in Waxiro. Consistent with previous studies in both wheat (Regina et al., 2006) and barley (Regina et al., 2010), down regulation of SBEIIb has only minor effects on starch structural and functional parameters. This result is markedly different from the situation in maize and rice where down regulation of SBEIIb is critical for generation of high amylose starches. These differences in genetic basis reflects differences in the relative expression levels of these isoforms in the various species; SBEIIa is expressed at low levels in the endosperms of maize (Gao, Fisher, Kim, Shannon, & Guiltinan, 1997) and rice (Yamanouchi & Nakamura, 1992), but at equal or higher levels than SBEIIb in barley (Sun, Sathish, Ahlandsberg, & Jansson, 1998) and wheat (Regina et al., 2005).

The *amo1* and ΔSBEIIa genotypes are characterised by intermediate values for most parameters between the control and high amylose groups. Two parameters were exceptions to this generalisation. Firstly, the *amo1* line has a very low λ_{max} value relative to the apparent amylose content of the starch. This observation is reflected in the absence of the Peak 3 shoulder eluting from SE-HPLC of the debranched starch. Secondly, despite the significant impact of the SBEIIa down-regulation on amylopectin chain length distribution in ΔSBEIIa, this starch retained an A-type crystallinity whereas ΔSBEIIa/ΔSBEIIb exhibited a B + V-type crystallinity. This suggests that amylopectin chain length distribution alone is not sufficient to predict crystalline polymorph, presumably because very high amylose levels interfere with or contribute to the process of molecular order. Further illustrating the unusual nature of the ΔSBEIIa starch is the observation that it has the highest 6′OH phosphate content of any of the starches measured in this study.

The three high amylose lines (*ssIIa*, *ssIIa/amo1* and ΔSBEIIa/ΔSBEIIb) are associated with low starch granule order and high amylose content; however, they differ markedly in relation to the amylopectin structural characteristics represented by the FACE DP 5–12 and DP 13–53 parameters, and the presence (ΔSBEIIa/ΔSBEIIb) or absence (*ssIIa*, *ssIIa/amo1*) of the Peak 3 shoulder on the amylopectin peak identified by SEC of debranched starch. Despite these differences in structure, amylose content measured by any of the three methods employed correlated closely with the resistant starch content determined for native starches similar to observation in rice (Butardo et al., 2011). Further studies will be required to test whether the correlation between amylose content and resistant starch content applies for these starches following the thermal and shear processes involved in food processing.

Analysis of the SE-HPLC traces of debranched starch revealed two structural features of interest. Firstly, a distinct shoulder region (denoted Peak 3) eluting at higher molecular weight ahead of the main amylopectin peak was observed for a number of starch genotypes as seen in other cereal species (Fitzgerald et al., 2009; Fuwa et al., 1999; Wang, White, Pollak, & Jane, 1993). This shoulder region is present in the wild type starches, reduced in *amo1* containing genotypes, and more prominent in lines with reduced SBEIIa and/or SBEIIb activity similar to SBEIIb downregulated rice starches (Butardo et al., 2011). Secondly, a second higher molecular weight peak (Peak 1) eluted ahead of the main amylose peak in high amylose starches. The reduction in Peak 3 in *amo1* containing starches may be reflecting the reduced proportion of chains of DP ≥ 37 in these starches, although not confirmed in this study through calibrating the molecular size elution from SE-HPLC to degree of polymerisation. Recently, *amo1* locus in barley is reported to be tightly linked to starch synthase *IIIa* gene (Li et al., 2011). SSIIIa mutations in maize and rice also lead to an amylopectin structure with decreased proportion of longer chains suggesting a role of SSIIIa in specifically elongating B2-B4 chains (Hanashiro, Higuchi, Aihara, Nakamura, & Fujita, 2011; Wang et al., 1993). Following GPC analyses, two additional investigations were conducted in order to clarify aspects of starch structure. Firstly, amylopectin and amylose pools (Pools 1 and 2 respectively) were generated for three genotypes, debranched, and subjected to SE-HPLC. This analysis confirmed that Pool 1 contained only the Peak 3 and Peak 4 fractions derived from high molecular weight amylopectin. The SE-HPLC analysis of debranched Pool 2 confirmed that the Peak 1 and Peak 2 are contained in this fraction, but also revealed significant quantities of Peak 3 and Peak 4 typical of amylopectin. This observation is consistent with the higher apparent amylose contents generated by GPC of undebranched starch compared to the SEC of debranched starch (Table 2). Three possibilities can be proposed to account for this result. Firstly, Pool 2 may contain low molecular weight amylopectin-like molecules generated by the biosynthetic process. Secondly, low molecular weight amylopectin molecules may be generated during starch isolation or as shear products during the GPC of undebranched starch. Thirdly, it is possible that the amylose molecules included in this study contain a population of short side chains more typical of the amylopectin fraction. Additional research is required to resolve these possibilities. Recently, 2D structural distribution analyses of amylose revealed its multimodal nature that depended on macromolecular sizes indicating a heterogeneous branching architecture unlike amylopectin for

which the branch length distributions are independent of macromolecular size (Vilaplana & Gilbert, 2010, 2011).

Three independent techniques have been used to investigate the higher order structure of the barley starches, ^{13}C CP/MAS, XRD and SAXS. Given that these techniques probe aspects of granule order and crystallinity, it is unsurprising that these parameters align closely with Principle Component 1. However, the plot of PC1 against PC2 shows that there are influences of amylopectin structure on the starch granule order parameters. The parameters XRD total crystallinity, SAXS Lamellar Peak Intensity, SAXS Lamellar Peak Width, XRD V-type, SAXS Lamellar Repeat Distance and NMR amorphous starch content are aligned with PC1, however, each of these parameters is also positively influenced by higher amylopectin A chain (FACE 5–12) content in the PC2 dimension. In contrast, the SAXS Peak Position and NMR double helical content are influenced by longer amylopectin chain length distribution. This result is consistent with previous studies showing that shorter chain length amylopectins found in waxy starches have higher total crystallinity, and higher perfection of the crystalline lattice (and thus more contrast with the amorphous regions of the granule) than starches with longer external chains. The result demonstrates that amylopectins with longer amylopectin external chains may contain greater helical content, but this does not translate into more crystallinity, or higher degrees of crystalline order. Total crystallinity and lamellar peak intensity were strongly inversely related to amylose content, consistent with the interpretation that as amylose content increases, a component of the amylose is present in crystalline regions of the granule where it disrupts crystalline arrays (Blazek & Gilbert, 2010).

The response of the barley starches to heating in water and shear was investigated using DSC and RVA analysis respectively. The DSC onset temperatures of *ssIIa* genotypes decreases relative to wild type, while for ΔSBEIIa/ΔSBEIIb, the genetic modification leads to a very broad peak rather than a peak with an increased onset temperature as is observed in maize (Tziotis, Seetharaman, Klucinec, Keeling, & White, 2005). It should be noted that for very high amylose starches, higher temperatures than 120 °C may be required to melt all of the double helices. This possibility remains open to future study although it should be noted that the endotherm returned to baseline levels by 120 °C for all starches. DSC Peak temperature and Gelatinisation End temperature were aligned with PC2 and longer chain amylopectin content rather than amylose content. Analysis of the RVA traits demonstrated that RVA Peak, RVA setback, RVA trough, RVA breakdown and RVA final show strong alignment to PC1 but are also the predominant functional parameter aligned with the weak PC3, for which this analysis only showed 6′OH phosphate as the potential structural feature aligning with this cluster of traits. Two RVA parameters, RVA Peak time and RVA pasting temperature, did not cluster tightly with the remaining RVA parameters, being more influenced by amylose content and granule disorder.

Resistant starch content was determined to investigate factors that influence the digestibility of the starch granule. However, it should be noted that the resistant starch values may not have physiological relevance in humans because the intact uncooked starch granules were assayed whereas the in vitro method is validated for foods as eaten. A very strong correlation between resistant starch content and amylose content was found, with the PCA analysis showing that RS was influenced by longer amylopectin chain lengths and low 6′OH phosphate content. This result confirms the observation, even for uncooked starches, that granule crystallinity is not correlated to resistant starch content. However, it should be noted that resistant starch content is not a measure of the initial stages of enzyme attack on starch granules, but rather a measure of the starch that remains undigested after prolonged enzymatic incubation. Future studies will investigate the factors determining resistant starch content of foods containing these barley genotypes.

5. Conclusions

The generation of a series of defined barley genotypes with amylose contents from 5 to 69% has provided the opportunity for a comprehensive analysis of the impact of increasing amylose content on a range of molecular, organisational and functional characteristics. The generation of starches with elevated amylose content by three independent genetic mechanisms (*amo*1, ssIIa and branching enzyme down-regulation) has provided a further opportunity to investigate the differential impact of each of these genetic and biochemical mechanisms for increasing amylose content on structure and functionality.

Acknowledgements

The authors acknowledge Suzhi Li for technical assistance with starch extraction and sample preparations for capillary electrophoresis and size exclusion chromatography, Christine Konik Rose for assistance with differential scanning calorimetry, Andrew Pedler for gel permeation chromatography and Sylvia Usher for resistant starch analysis.

Appendix A. Supplementary data

Supplementary data associated with this article can be found, in the online version, at http://dx.doi.org/10.1016/j.carbpol.2012.04.054.

References

Bailey, J. M., & Whelan, W. J. (1961). Physical properties of starch, 1. Relationship between iodine stain and chain length. *Journal of Biological Chemistry*, *236*(4), 969–973.
Bertoft, E. (2004). On the nature of categories of chains in amylopectin and their connection to the super helix model. *Carbohydrate Polymers*, *57*(2), 211–224.
Bertoft, E. (2007). Composition of clusters and their arrangement in potato amylopectin. *Carbohydrate Polymers*, *68*(3), 433–446.
Bertoft, E., Kallman, A., Koch, K., Andersson, R., & Aman, P. (2011). The cluster structure of barley amylopectins of different genetic backgrounds. *International Journal of Biological Macromolecules*, *49*(4), 441–453.
Bertoft, E., Piyachomkwan, K., Chatakanonda, P., & Sriroth, K. (2008). Internal unit chain composition in amylopectins. *Carbohydrate Polymers*, *74*(3), 527–543.
Biliaderis, C. G., Page, C. M., Slade, L., & Sirett, R. R. (1985). Thermal behavior of amylose–lipid complexes. *Carbohydrate Polymers*, *5*(5), 367–389.
Bird, A. R., Usher, S., May, B., Topping, D. L., & Morell, M. K. (2012). Resistant starch—Measurement, intakes and dietary targets. In S. S. Cho (Ed.), *Dietary fiber—Proceedings of the Vahouny Symposium*. NY: CRC Press.
Blazek, J., & Gilbert, E. P. (2010). Effect of enzymatic hydrolysis on native starch granule structure. *Biomacromolecules*, *11*(12), 3275–3289.
Blazek, J., & Gilbert, E. P. (2011). Application of small-angle X-ray and neutron scattering techniques to the characterisation of starch structure: A review. *Carbohydrate Polymers*, *85*(2), 281–293.
Blazek, J., Salman, H., Rubio, A. L., Gilbert, E., Hanley, T., & Copeland, L. (2009). Structural characterization of wheat starch granules differing in amylose content and functional characteristics. *Carbohydrate Polymers*, *75*(4), 705–711.
Bogracheva, T. Y., Morris, V. J., Ring, S. G., & Hedley, C. L. (1998). The granular structure of C-type pea starch and its role in gelatinization. *Biopolymers*, *45*(4), 323–332.
Borén, M., Glaring, M. A., Ghebremedhin, H., Olsson, H., Blennow, A., & Jansson, C. (2008). Molecular and physicochemical characterization of the high-amylose barley mutant Amo1. *Journal of Cereal Science*, *47*(1), 79–89.
Buléon, A., Colonna, P., Planchot, V., & Ball, S. (1998). Starch granules: Structure and biosynthesis. *International Journal of Biological Macromolecules*, *23*(2), 85–112.
Butardo, V. M., Fitzgerald, M. A., Bird, A. R., Gidley, M. J., Flanagan, B. M., Larroque, O., et al. (2011). Impact of down-regulation of starch branching enzyme IIb in rice by artificial microRNA- and hairpin RNA-mediated RNA silencing. *Journal of Experimental Botany*, *62*(14), 4927–4941.
Campbell, M. R., White, P. J., & Pollak, L. M. (1994). Dosage effect at the sugary-2 locus on maize starch structure and function. *Cereal Chemistry*, *71*(5), 464–468.
Fitzgerald, M. A., Bergman, C. J., Resurreccion, A. P., Moller, J., Jimenez, R., Reinke, R. F., et al. (2009). Addressing the dilemmas of measuring amylose in rice. *Cereal Chemistry*, *86*(5), 492–498.
Fuwa, H., Glover, D. V., Fujita, S., Sugimoto, Y., Inouchi, N., Sugihara, M., et al. (1999). Structural and physicochemical properties of endosperm starches possessing

different alleles at the amylose-extender and waxy locus in maize (*Zea mays* L.). *Starch-Starke*, *51*(5), 147–151.
Gao, J., Vasanthan, T., & Hoover, R. (2009). Isolation and characterization of high-purity starch isolates from regular, waxy, and high-amylose Hulless barley grains. *Cereal Chemistry*, *86*(2), 157–163.
Gao, M., Fisher, D. K., Kim, K. N., Shannon, J. C., & Guiltinan, M. J. (1997). Independent genetic control of maize starch-branching enzymes IIa and IIb—Isolation and characterization of a Sbe2a cDNA. *Plant Physiology*, *114*(1), 69–78.
Hanashiro, I., Higuchi, T., Aihara, S., Nakamura, Y., & Fujita, N. (2011). Structures of starches from rice mutants deficient in the starch synthase isozyme SSI or SSIIIa. *Biomacromolecules*, *12*(5), 1621–1628.
Hizukuri, S. (1986). Polymodal distribution of the chain lengths of amylopectins, and its significance. *Carbohydrate Research*, *147*(2), 342–347.
Imberty, A., & Perez, S. (1988). A revisit to the 3-dimensional structure of B-type starch. *Biopolymers*, *27*(8), 1205–1221.
Jenkins, P. J., & Donald, A. M. (1995). The influence of amylose on starch granule structure. *International Journal of Biological Macromolecules*, *17*(6), 315–321.
Kubo, A., Yuguchi, Y., Takemasa, M., Suzuki, S., Satoh, H., & Kitamura, S. (2008). The use of micro-beam X-ray diffraction for the characterization of starch crystal structure in rice mutant kernels of waxy, amylose extender, and sugary1. *Journal of Cereal Science*, *48*(1), 92–97.
Li, J. -H, Guiltinan, M. J., & Thompson, D. B. (2007). Mutation of the maize sbela and ae genes alters morphology and physical behavior of wx-type endosperm starch granules. *Carbohydrate Research*, *342*(17), 2619–2627.
Li, L., Jiang, H. X., Campbell, M., Blanco, M., & Jane, J. L. (2008). Characterization of maize amylose-extender (ae) mutant starches, Part I: Relationship between resistant starch contents and molecular structures. *Carbohydrate Polymers*, *74*(3), 396–404.
Li, Z., Li, D., Du, X., Wang, H., Larroque, O., Jenkins, C. L. D., et al. (2011). The barley amo1 locus is tightly linked to the starch synthase IIIa gene and negatively regulates expression of granule-bound starch synthetic genes. *Journal of Experimental Botany*, *62*(14), 5217–5231.
Lopez-Rubio, A., Flanagan, B. M., Gilbert, E. P., & Gidley, M. J. (2008). A novel approach for calculating starch crystallinity and its correlation with double helix content: A combined XRD and NMR study. *Biopolymers*, *89*(9), 761–768.
Matsuki, J., Yasui, T., Sasaki, T., Fujita, M., & Kitarnura, Y. (2008). Effects of the barley amo1 and wax genes on starch structure and physicochemical properties. *Starch-Starke*, *60*(6), 279–285.
Merritt, N. R. (1967). A new strain of barley-M with starch of high amylose content. *Journal of the Institute of Brewing*, *73*(6), 583–585.
Morell, M. K., Kosar-Hashemi, B., Cmiel, M., Samuel, M. S., Chandler, P., Rahman, S., et al. (2003). Barley sex6 mutants lack starch synthase IIa activity and contain a starch with novel properties. *Plant Journal*, *34*(2), 173–185.
Morrison, W. R., Law, R. V., & Snape, C. E. (1993). Evidence for inclusion complexes of lipids with V-amylose in maize, rice and oat starches. *Journal of Cereal Science*, *18*(2), 107–109.
Morrison, W. R., Tester, R. F., Snape, C. E., Law, R., & Gidley, M. J. (1993). Swelling and gelatinization of cereal starches, 4. Some effects of lipid-complexed amylose and free amylose in waxy and normal barley starches\. *Cereal Chemistry*, *70*(4), 385–391.
O'Shea, M. G., Samuel, M. S., Konik, C. M., & Morell, M. K. (1998). Fluorophore-assisted carbohydrate electrophoresis (FACE) of oligosaccharides: Efficiency of labelling and high-resolution separation. *Carbohydrate Research*, *307*(1–2), 1–12.
Regina, A., Bird, A., Topping, D., Bowden, S., Freeman, J., Barsby, T., et al. (2006). High-amylose wheat generated by RNA interference improves indices of large-bowel health in rats. *Proceedings of the National Academy of Sciences of the United States of America*, *103*(10), 3546–3551.
Regina, A., Kosar-Hashemi, B., Li, Z. Y., Pedler, A., Mukai, Y., Yamamoto, M., et al. (2005). Starch branching enzyme IIb in wheat is expressed at low levels in the endosperm compared to other cereals and encoded at a non-syntenic locus. *Planta*, *222*(5), 899–909.
Regina, A., Kosar-Hashemi, B., Ling, S., Li, Z. Y., Rahman, S., & Morell, M. (2010). Control of starch branching in barley defined through differential RNAi suppression of starch branching enzyme IIa and IIb. *Journal of Experimental Botany*, *61*(5), 1469–1482.
Schondelmaier, J., Jacobi, A., Fischbeck, G., & Jahoor, A. (1992). Genetic-studies on the mode of inheritance and localization of the Amo1 (high amylose) gene in barley. *Plant Breeding*, *109*(4), 274–280.
Song, Y., & Jane, J. (2000). Characterization of barley starches of waxy, normal, and high amylose varieties. *Carbohydrate Polymers*, *41*(4), 365–377.
Sun, C. X., Sathish, P., Ahlandsberg, S., & Jansson, C. (1998). The two genes encoding starch-branching enzymes IIa and IIb are differentially expressed in barley. *Plant Physiology*, *118*(1), 37–49.
Tan, I., Flanagan, B. M., Halley, P. J., Whittaker, A. K., & Gidley, M. J. (2007). A method for estimating the nature and relative proportions of amorphous, single, and double-helical components in starch granules by C-13 CP/MAS NMR. *Biomacromolecules*, *8*(3), 885–891.
R Development Core Team (Ed.). (2009). *R: A Language and Environment for Statistical Computing*. Vienna, Austria: R Foundation for Statistical Computing.
Tziotis, A., Seetharaman, K., Klucinec, J. D., Keeling, P., & White, P. J. (2005). Functional properties of starch from normal and mutant corn genotypes. *Carbohydrate Polymers*, *61*(2), 238–247.
Vilaplana, F., & Gilbert, R. G. (2010). Two-dimensional size/branch length distributions of a branched polymer. *Macromolecules*, *43*(17), 7321–7329.
Vilaplana, F., & Gilbert, R. G. (2011). Analytical methodology for multidimensional size/branch-length distributions for branched glucose polymers using off-line 2-dimensional size-exclusion chromatography and enzymatic treatment. *Journal of Chromatography A*, *1218*(28), 4434–4444.
Waduge, R. N., Hoover, R., Vasanthan, T., Gao, J., & Li, J. (2006). Effect of annealing on the structure and physicochemical properties of barley starches of varying araylose content. *Food Research International*, *39*(1), 59–77.
Wang, Y. J., White, P., Pollak, L., & Jane, J. (1993). Characterization of starch structures of 17 maize endopserm mutant genotypes with OH43 inbred line background. *Cereal Chemistry*, *70*(2), 171–179.
Wu, H. C. H., & Sarko, A. (1978). Packing analysis of carbohydrates and polysaccharides, 9. Double-helical molecular structure of crystalline A-Amylose. *Carbohydrate Research*, *61*(March), 27–40.
Yamanouchi, H., & Nakamura, Y. (1992). Organ specificity of isoforms of starch branching enzyme (Q-enzyme) in rice. *Plant and Cell Physiology*, *33*(7), 985–991.
Yao, Y., Thompson, D. B., & Guiltinan, M. J. (2004). Maize starch-branching enzyme isoforms and amylopectin structure. In the absence of starch-branching enzyme IIb, the further absence of starch-branching enzyme Ia leads to increased branching. *Plant Physiology*, *136*(3), 3515–3523.
Yasui, T., Ashida, K., & Sasaki, T. (2009). Chain-length distribution profiles of amylopectin isolated from endosperm starch of waxy and low-amylose bread wheat (*Triticum aestivum* L.) lines with common genetic background. *Starch-Stärke*, *61*(12), 677–686.